HHS Public Access

Author manuscript

Clin Cancer Res. Author manuscript; available in PMC 2018 August 15.

Published in final edited form as:

Clin Cancer Res. 2017 August 15; 23(16): 4680–4692. doi:10.1158/1078-0432.CCR-16-3029.

Feasibility of ultra-high-throughput functional screening of melanoma biopsies for discovery of novel cancer drug combinations

Adam A. Friedman[1,2], **Yun Xia**[2,3], **Lorenzo Trippa**[4], **Long Phi Le**[1], **Vivien Igras**[1,2], **Dennie T. Frederick**[1], **Jennifer A. Wargo**[1,5,6], **Kenneth K. Tanabe**[1,5], **Donald P. Lawrence**[1], **Donna S. Neuberg**[4], **Keith T. Flaherty**[1], and **David E. Fisher**[1,2]

[1]Massachusetts General Hospital Cancer Center, Harvard Medical School, Boston, Massachusetts, USA

[2]Dermatology and Cutaneous Biology Research Center, Massachusetts General Hospital, Charlestown, Massachusetts, USA

[3]Department of Plastic Surgery, Union Hospital, Tongji Medical College, Huazhong University of Science and Technology, Wuhan 430022, China

[4]Department of Biostatistics and Computational Biology, Dana-Farber Cancer Institute, Boston, Massachusetts, USA

[5]Division of Surgical Oncology, Massachusetts General Hospital, Charlestown, Massachusetts, USA

Abstract

Purpose—Successful development of targeted therapy combinations for cancer patients depends on first discovering such combinations in predictive preclinical models. Stable cell lines and mouse xenograft models can have genetic and phenotypic drift and may take too long to generate to be useful as a personalized medicine tool.

Experimental Design—To overcome these limitations, we have used a platform of ultra-high-throughput functional screening of primary biopsies preserving both cancer and stroma cell populations from melanoma patients to nominate such novel combinations from a library of thousands of drug combinations in a patient-specific manner within days of biopsy. In parallel, patient-derived xenograft (PDX) mouse models were created and novel combinations tested for their ability to shrink matched patient-derived tumors.

Results—The screening method identifies specific drug combinations in tumor cells with patterns that are distinct from those obtained from stable cell lines. Screening results were highly specific to individual patients. For patients with matched PDX models, we confirmed that individualized novel targeted therapy combinations could inhibit tumor growth. In particular, a combination of multi-kinase and PI3K/Akt inhibitors was effective in some BRAF-wild-type

Corresponding Author: David E. Fisher, Dermatology and Cutaneous Biology Research Center, Massachusetts General Hospital, Bartlett 6, 55 Fruit Street, Boston, MA 02114; Phone: 617-643-5428; Fax: 617-643-6588; dfisher3@partners.org.

[6]Current address: Departments of Genomic Medicine and Surgical Oncology, University of Texas M.D. Anderson Cancer Center, Houston, Texas, USA.

melanomas, and the addition of cediranib to the BRAF inhibitor PLX4720 was effective in a PDX model with *BRAF* mutation.

Conclusions—This proof-of-concept study demonstrates the feasibility of using primary biopsies directly for combinatorial drug discovery, complementing stable cell lines and xenografts, but with much greater speed and efficiency. This process could potentially be used in a clinical setting to rapidly identify therapeutic strategies for individual patients.

Keywords

melanoma; combinations; BRAF; models; personalized

Introduction

Cancer cells develop resistance to single agents through selection of minor clones or epigenetic adaptation (1–4). Combinations of targeted agents can provide deeper and more lasting benefit to patients, for example in melanoma (5) or breast cancer (6). Combination strategies have been discovered through functional genomics (7) or unbiased combinatorial drug screening in cell lines, as we have recently reported (8).

The preclinical models used for screen-based functional studies are limited by their inadequate representation of the genetics and microenvironment of the original tumor (9). Stable cell lines have adapted to plastic cell culture conditions, with genetic drift and altered drug sensitivity (10, 11). Furthermore, certain tissue subtypes are not amenable to cell line generation, such as prostate cancer. Patient-derived xenografts (PDX) can require months to generate sufficient tumor material for drug testing for personalized medicine (12, 13) and demonstrate genetic drift during cultivation (14). Such testing is necessarily resource-limited to a small number of drugs.

An ideal cancer model would enable rapid, scalable screening to test a large number of drug conditions and recapitulate the tumor microenvironment and genetics. Direct functional analysis of living patient biopsies, i.e., chemosensitivity testing, provides such an approach by enabling functional analysis of unmodified patient cancer cells within days of biopsy, in an automated and high-throughput manner (15). For hematological malignancies, this approach has been explored for both drug discovery and personalized therapeutic matching (16, 17). In solid tumors, however, few studies have validated that such an approach can be used for drug discovery or help identify novel combinations of targeted agents. In this proof-of-concept study, we describe an ultra-high-throughput screening platform for identification of novel drug combinations using primary biopsies from patients with melanoma and validated several of these novel, clinically-actionable combinations in paired PDX models. Such screening could be used as a new tool for drug development and personalized cancer therapeutic matching.

Patients and Methods

Melanoma patient tumor samples

De-identified biopsies of patients were obtained after informed consent on Dana-Farber/Harvard Cancer Center Institutional Review Board (IRB)-approved protocols 11–181 and 02–017 in accordance with the Declaration of Helsinki. Single-cell suspensions from each biopsy were obtained after mechanical and enzymatic dissociation as previously described (18), red blood cells were lysed (RBC Lysis Buffer, BioLegend) and resuspended in RPMI 1640 media containing 10% fetal bovine serum.

Ultra-high-throughput combinatorial drug screen

Approximately 500 cells from each biopsy were seeded in each well of 1,536-well microtiter plates (PerkinElmer) and incubated overnight. Combinatorial drug library was pin-transferred to the seeded plates as previously described (8). Plates were incubated for 96 hours, fixed in 4% formaldehyde, washed in PBS containing 0.1% Triton (PBST), and incubated overnight with antibodies (1:200) to S100 (Dako). The plates were then washed twice, incubated with Alexa 488 secondary antibodies (1:1000, Life Technologies) and DAPI 2–16 hours, and washed with PBST. Plates were then imaged using the CellWorX high-throughput microscope (Applied Precision Inc.) and nuclei and cells with S100 staining were counted with the Multi-Wavelength Cell Scoring module of the MetaExpress image analysis software (Molecular Devices). Representative control well images from each sample were manually reviewed to confirm S100 staining corresponded to cells with melanoma morphology. Technical replicates were averaged. Where replicates were available, Z' scores were calculated (19), varying from 0.15 for CBRC029 to 0.58 for CBRC056.

Xenografts

For mouse xenotransplant experiments, 5×10^6 to 1×10^7 cells of single cell suspensions from the primary patient biopsies, suspended in 25% Matrigel (Corning), were injected subcutaneously into the flank of female NSG mice aged to 7–8 weeks, and subsequently expanded to additional animals until the second or third generation. After tumors reached 100–150 mm^3 in size, animals were randomized to treatment groups as described below. Mice were given *ad libitum* mouse chow, or, for those bearing tumor CBRC026 and randomized to PLX4720 treatment, mouse chow containing 2% PLX4720 as described (20). All studies and procedures involving animal subjects were approved by the Institutional Animal Care and Use Committees of Massachusetts General Hospital and were conducted strictly in accordance with the approved animal handling protocol. Tumor volume was calculated by the formula ½ × (length × $width^2$), measured by digital calipers. PLX4720 mouse chow was generously supplied by Plexxikon Inc. Compounds for *in vivo* dosing were obtained from DC Chemicals (Shanghai, China). Compound dosing amounts, route, and formulation, were obtained from published studies, as follows: cediranib (6mg/kg) was administered by oral gavage daily (21); bortezomib (1mg/kg) was given by intraperitoneal injection twice weekly (22); vatalanib (50mg/kg) by oral gavage daily (23); CX4945 (75mg/kg) by oral gavage twice daily (24); perifosine (36mg/kg) oral gavage daily (25); YM155 (4mg/kg) by intraperitoneal injection daily (26); XL147 (100mg/kg) by oral gavage

daily (27); R788 (40mg/kg) by oral gavage twice daily (28); fingolimod (25mg/kg) by oral gavage daily (29); dasatinib (70mg/kg) by oral gavage daily (30); and tozasertib (75mg/kg) by intraperitoneal injection daily (31).

Next generation sequencing

NGS was implemented using the multiplex polymerase chain reaction (PCR) technology Anchored Multiplex PCR (AMP) for single nucleotide variant (SNV) and insertion/deletion (indel) detection in genomic DNA, as previously described (32). Briefly, genomic DNA was isolated from a formalin-fixed paraffin embedded tumor specimen or single-cell suspension. The genomic DNA was sheared with the Covaris M220 instrument, followed by end-repair, adenylation, and ligation with an adapter. A sequencing library targeting hotspots and exons in 39 genes was generated using two hemi-nested PCR reactions. Illumina MiSeq 2 × 147 base paired-end sequencing results were aligned to the hg19 human genome reference using BWA-MEM (33). MuTect (34) and a laboratory-developed insertion/deletion analysis algorithm were used for SNV and indel variant detection, respectively (32). This assay has been validated to detect SNV and indel variants at 5% allelic frequency or higher in target regions with sufficient read coverage.

The gene targets covered by this assay are as follows (exons): AKT1 (3), ALK (22, 23, 25), APC (16), BRAF (11, 15), CDH1 (1, 2, 3, 4, 5, 6, 7, 8, 9, 10, 11, 12, 13, 14, 15, 16), CDKN2A (1, 2, 3), CTNNB1 (3), DDR2 (12, 13, 14, 15, 16, 17, 18), EGFR (7, 15, 18, 19, 20, 21), ERBB2 (10, 20), ESR1 (8), FBXW7 (1, 2, 3, 4, 5, 6, 7, 8, 9, 10, 11), FGFR1 (4, 8, 15, 17), FGFR2 (7, 9, 12,14), FGFR3 (7, 8, 9, 14, 16), FOXL2 (1), GNA11 (5), GNAQ (4, 5), GNAS (6, 7, 8, 9), HRAS (2, 3), IDH1 (3, 4), IDH2 (4), KIT (8, 9, 11, 17), KRAS (2, 3, 4, 5), MAP2K1 (2, 3), MET (14, 16, 19, 21), NOTCH (25, 26, 34), NRAS (2, 3, 4, 5), PDGFRA (12, 14, 18, 23), PIK3CA (2, 5, 8, 10, 21), PIK3R1 (1, 2, 3, 4, 5, 6, 7, 8, 9, 10), PTEN (1, 2, 3, 4, 5, 6, 7, 8, 9), RET (11, 16), ROS1 (38), SMAD4 (2, 3, 4, 5, 6, 7, 8, 9, 10, 11, 12), SMO (9), STK11 (1, 2, 3, 4, 5, 6, 7, 8, 9), TP53 (1, 2, 3, 4, 5, 6, 7, 8, 9, 10, 11), and VHL (1, 2, 3).

Combination selection algorithm

We model the variations of cancer cells (in log-ratio scale) $D_{i,j}$, where i indexes the sample and j the agents' combination:

$$D_{i,j}=T_1(j)+T_2(j)+T_{1,2}(j)+\varepsilon.$$

Here $T_1(j)$ and $T_2(j)$ are the main effects of the two agents in combination j, while the third regression component $T_{1,2}(j)$ captures the interaction and possible synergy between the two drugs in the j-th combination.

The number of main effects $T_1(j)$, $T_2(j)$ to be inferred is equal to the number of agents involved in the experiment, while the number of interaction terms $T_{1,2}(j)$ increases quadratically with the number of agents. We therefore used standard penalized regression (35) and shrink the $T_{1,2}(j)$ estimates toward zero.

A nearly identical model is estimated separately for the variation of stromal cell counts

$$D^S_{i,j}=T^S_1(j)+T^S_2(j)+T^S_{1,2}(j)+\varepsilon.$$

The prediction components ($T_1(j)+T_2(j)+T_{1,2}(j)$), $\left(T^S_1(j)+T^S_2(j)+T^S_{1,2}(j)\right)$ and the interaction terms $T_{1,2}(j)$ are used to rank combinations. We first drop the combinations with toxicities $\left(T^S_1(j)+T^S_2(j)+T^S_{1,2}(j)\right)$ above the median. Then the remaining ones are raked accordingly to a weighted combination of ($T_1(j)+T_2(j)+T_{1,2}(j)$) and $T_{1,2}(j)$.

For CBRC056, a second algorithm was used to identify the bortezomib and CX4945 combination. Here, drug combinations were given a combined score based on specific thresholds of parameters: S100− cell count % control > 70%, S100+ cell count < 70%, and Bliss synergy > 40%, where each result is given a score of “1” if true and the score summed for each concentration; finally, the combinations were ranked by the sum score.

Other statistical analyses

All statistical tests excluding those explicitly discussed above were implemented using GraphPad Prism 6 for Mac (GraphPad). When used, Student’s *t*-test (two-sided) was implemented after confirming equal variance by *F* test. Heat maps, hierarchical clustering, and SAM analysis were implemented using the MeV platform (36).

Results

We previously created a diverse combinatorial drug library for use in a high-throughput combinatorial viability screen in melanoma cell lines and short-term cultures (8). This library included a range of drug classes: signal transduction inhibitors, cell cycle regulators, epigenetic modulators, and cytotoxic chemotherapies. We tested a portion of this drug library selected for translational relevance by biasing towards drugs currently under clinical development (2,850 drug combinations from 76 single drugs) to discover effective drug combinations in primary patient biopsies from ten patients at our institution (Table 1). Biopsy samples were screened as described in ultra-high-throughput 1,536-well format plates. Patient biopsies were genotyped using a variety of methods dependent on clinical practice at the time of biopsy: $BRAF^{V600E/K}$-only testing, SnapShot sequencing (37) for 13 known oncogenic drivers, to wider hotspot sequencing using next generation sequencing (NGS) (32).

Patient biopsies are a highly heterogeneous mixture of tumor cells and stromal components including cancer-associated fibroblasts, normal epithelial cells, and inflammatory cells. Previous methods relying on bulk scoring of cell viability may not accurately reflect effects on the tumor cell population specifically. By staining the samples prior to imaging with antibodies to S100, a melanoma marker present in > 95% of cases (38) and using automated imaging and scoring algorithms, we could then segment the cell subpopulations into melanoma (S100+) and stromal (S100−) groups (Fig. 1A). This allowed us to observe melanoma-specific cell viability versus non-melanoma cell effects, providing a selectivity

score. S100 positivity (tumor cell content) ranged from 10% (CBRC002) to 95% (CBRC056). This segmentation was critical for distinguishing melanoma-specific drug effects, as we found little correlation between effects on melanoma and admixed non-melanoma cells (Supplementary Fig. 1A) or between the S100+ segmented and non-segmented entire population in biopsies with stromal contribution (e.g., CBRC007, Fig. 1B). Drugs with specific effects on tumor populations with no cytotoxic effect on normal, non-pathogenic stroma may be more desirable for patient use.

For each drug combination treatment, we collected these melanoma and stromal cell counts, extracted their ratio (selectivity) and synergy (Bliss independence), and normalized the values to DMSO (full data provided in Supplementary Table 1). Technical replication of a biopsy screened in parallel (CBRC056, Fig. 1C) showed a Z' score (19) of 0.58 and excellent correlation between drug effects overall ($R = 0.8$, $P < 0.0001$) and the top-ranked anti- or pro-proliferative agents (Fig. 1C, bar graph). Biological replicates of CBRC029 (Fig. 1D) showed that drugs with strong viability (fingolimod, a partial agonist of SP1R; BRAF inhibitor PLX4720) or pro-survival (DNA methyltransferase inhibitor decitabine) effects showed similar relative ranking, with overall correlation $R = 0.5$, $P < 0.0001$. Pearson correlation coefficient of drug effects within multiple replicates of the same patient biopsy was significantly higher than between different patients' biopsies for both single drugs (0.44 vs 0.16, $P = 4.5 \times 10^{-13}$, Student's t test) and drug combinations (0.4 vs 0.13, $P = 7.1 \times 10^{-17}$, Student's t test) (Supplementary Fig. 1B). BRAF mutant melanoma biopsy cells displayed a trend towards greater sensitivity to BRAF inhibitor PLX4720 than BRAF wild-type melanoma biopsy cells (Fig. 1E, $P = 0.08$, Student's t-test), as expected (3), despite purposeful use of a low concentration of the inhibitor. These results suggested that the output from the biopsy screening was reflective of biologically meaningful perturbation of cell number.

Drug effects in primary patient biopsies

We compared the melanoma-cell specific effects of drugs in our library across the ten patient biopsies by hierarchical clustering of the viability data. Broad viability effects in most biopsies were seen with the proteasome inhibitor bortezomib, the pro-apoptotic B-cell lymphoma 2 (BCL2) family member inhibitor ABT263, HER2 and EGFR inhibitor lapatinib, the PDK1 inhibitor OSU03012, and combinations containing fingolimod; increased cell count was seen with the Aurora kinase inhibitor tozasertib, decitabine, and combinations containing the JAK inhibitor tofacitinib (Figs. 2A and 2B). This latter activity may be due to pro-proliferative activity or anti-apoptotic activity in the freshly isolated cells which were mostly non-proliferative during our four-day assay.

As we previously described in large-scale melanoma cell line screening (8), we also observed heterogeneity of the drug combination effects across primary patient biopsies. Interestingly, while the median effect of any individual combination was clustered near ~100% control effects, the minimum effect of any given combination was significantly lower, and 48% of drug combinations caused a > 30% reduction in melanoma cell counts in at least one patient biopsy (Fig. 2C); nearly 20% of drug combinations caused > 50%

melanoma cell count loss in at least one biopsy. These data suggest individual patients may have a wide array of potentially effective and highly personalized drug combinations.

Comparison between cell lines and primary patient biopsies

We compared our biopsy data to our previous screen of the same library in stable melanoma cell lines (8). In general, individual drugs and their combinations had stronger viability effects in cell lines than primary biopsies ($P = 0.0001$ for both, Student's *t*-test) with an average ratio of median effects of a given drug combination in cell lines compared to biopsies of 0.82 +/− 0.18 (Fig. 3A).

Next, we used the statistical analysis of microarray (SAM) approach (39) to identify drugs with significantly different effects in cell lines compared to patient biopsies. Both bortezomib and fingolimod decreased cell viability in stable cell lines and melanoma biopsies (Fig. 3B). Tozasertib and decitabine reduced stable cell line viability but induced melanoma cell counts in patient biopsies. Other individual drugs with effects on cell lines but not biopsies included cytotoxic chemotherapies such as gemcitabine, cisplatin, and vincristine, as well as signaling inhibitors such as the Raf inhibitor CHIR-265 and dasatinib. A large number of drug combinations showed significantly stronger effects in cell lines compared to primary biopsies, including many containing the microtubule inhibitor docetaxel (Fig. 3C). In contrast, combinations including the JNK inhibitor BI78D3 or p21 activated kinase (PAK) inhibitor IPA3 showed more viability effects in primary biopsy melanoma cells than in cell lines.

For one of the patient biopsies, we generated a stable, homogenous short-term culture (CBRC013). Even within this same patient background, we found differences in the previously reported drug responses in the short-term culture (8) compared to the original patient biopsy (Supplementary Fig. 1C). For example, while bortezomib and ABT263 affected cell viability in both samples, and decitabine and the sirtuin-1 inhibitor EX527 increased cell count in both samples, the cytotoxic STA4783 and ROCK inhibitor RKI983 affected the primary biopsy more than the short-term culture and CHIR265 and PLK inhibitor BI2536 had stronger viability effect in the short-term culture. Thus even short-term cultures with homogenous tumor-only populations may exhibit discrepant behaviors relative to mixed tumor populations, where normal epithelial, cancer associated fibroblasts, and infiltrating lymphocytes modulate drug responses.

Prediction of *in vivo* combination efficacy by *ex vivo* functional profiling

We next tested whether primary patient biopsy screening would be predictive of *in vivo* results. We used matched PDX mouse models derived from the same screened biopsy at passages 2–3 for five of these patient biopsies to validate key screening results.

Novel functional screening algorithm—To choose amongst the >2,800 combinations tested in the biopsies, we developed an algorithm to rank drug combinations (see Methods). The input parameters for this algorithm included the absolute melanoma (S100+) cell count, selectivity versus stromal cell count, and synergy between the two drugs in the melanoma population. The ranking algorithm has three main components. First, it eliminates all

combinations associated with risk of toxicities: all combinations with (i) individual stromal cell count or (ii) average stroma cell count across samples, below the median of control do not appear in the final ranking. Second, using penalized regression modeling (35), the algorithm predicts, for each sample and drug combination, the difference between tumor cell count and stromal cell count, at low and high doses. These predictions identify hypothetical additional technical replicates beyond the available data. Third, it creates a consensus rank which summarizes the two ranks indicated.

Given the inevitable noise in any screening system, we assumed that this ranking provided a guide as to the effectiveness of a particular combination, but that it would be unlikely to distinguish within the top 10–20 out of thousands of combinations. We therefore selected combinations for *in vivo* testing manually within the top combinations using compound commercial availability, oral bioavailability, and overall degree of literature validation of animal dosing, PK-PD relationship, and anti-tumor effectiveness in other systems. This allowed us to test a previously-described starting dose, more quickly addressing the feasibility of using the screening results for potential rapid deployment.

***In vivo* validation of *ex vivo* screening—**For all five melanoma samples tested in PDX models, we observed one or more additive, if not synergistic, reductions in melanoma tumor growth in animals caused by the *ex vivo*-discovered combinations. For two patients, the Syk and multi-kinase inhibitor R406/R788 appeared in top-ranked combinations along with inhibitors of the PI3K/Akt pathway. For patient CBRC013, combination with the PI3K inhibitor XL147 was highly ranked (Supplementary Fig. 2A) and significantly suppressed growth of the tumor compared to control, while neither single agent had significant effects ($P = 0.04$ by one-way ANOVA with Dunnett's multiple comparison test) (Fig. 4A, Supplementary Fig. 2B). Bliss synergy score between the two drugs *in vivo* (29%) was similar to that observed *ex vivo* (25%). For patient CBRC029, we validated a synergistic interaction *in vivo* between R788 and perifosine, an Akt inhibitor, with 18% Bliss synergy. Perifosine alone or combined with R788-treated animals reduced tumor size compared to control ($P = 0.004$ and $P = 0.0007$, one-way ANOVA with Dunnett's multiple comparison test) (Fig. 4B, Supplementary Fig. 2D). Several other highly ranked combinations identified *ex vivo* for CBRC029 (Supplementary Fig. 2C) showed strong synergistic activity in reducing the growth of CBRC029 xenografts. The combination of perifosine and fingolimod reduced tumor growth significantly more than perifosine alone (Fig. 4C, $P < 0.02$, Student's *t*-test) and increased the progression-free survival (PFS) of the perifosine and fingolimod combination-treated animals compared to perifosine- only treated animals (Supplementary Fig. 2E, $P = 0.03$, log-rank test). Dasatinib and dasatinib combined with tozasertib reduced tumor size compared to control (Fig. 4D, $P = 0.0001$ and $P = 0.0001$, one-way ANOVA with Tukey's multiple comparison test), and the drug combination increased PFS compared to dasatinib-treated animals (Supplementary Fig. 2F, $P = 0.02$ by log-rank test).

BRAF inhibitor combinations—For melanoma patients whose tumors harbor activating mutations in the oncogene BRAF, inhibitors of BRAF alone such as PLX4720 and in combination with MEK inhibitors are standard of care therapy. We investigated whether novel combinations with the BRAF inhibitor backbone could be identified for individual

BRAF-mutant patients. Three of the five tumors we tested *in vivo* were identified to have *BRAF* mutations (CBRC026, CBRC056, and CBRC058). Surprisingly, for only one tumor (CBRC026) was PLX4720 identified in a highly-ranked combination. For the other two tumors (CBRC056 and CBRC058), PLX4720 was not highly ranked, implying that other drugs may be *relatively* more active for these patients than BRAF inhibitors, which can have heterogeneous and often partial responses in the clinic.

For tumor CBRC056, highly-ranked combinations often contained the proteasome inhibitor bortezomib (Supplementary Fig. 3A). The combination of the VEGFR inhibitor vatalanib and bortezomib reduced tumor growth synergistically and significantly more than either drug alone (Fig 5A, $P = 0.003$ for both comparisons by Student's *t*-test). Because of weight loss with this combination, using an alternative algorithm we identified a novel combination between bortezomib with the CK2 inhibitor CX4945 as active *ex vivo* (Supplementary Fig. 3B). This combination reduced the growth of CBRC056 PDX tumors, with a Bliss synergy of 14%, equal to the *ex vivo* synergy of 14% seen at high dose *ex vivo* (Fig. 5B). The combination of bortezomib and CX4945 reduced tumor growth significantly more than either drug alone ($P = 0.0001$ and $P = 0.01$, respectively by Student's *t*-test), and significantly reduced tumor progression compared to CX4945-treated animals (Supplementary Fig. 3B, $P = 0.02$, log-rank test). For tumor CBRC058, the survivin inhibitor YM155 appeared in multiple top-ranked combinations, including one with perifosine (Supplementary Fig. 3C). Both YM155 and perifosine had strong single-agent activity *in vivo* not predicted by the *ex vivo* data but there was additional *in vivo* activity when combined (Fig. 5C). We explored whether PLX4720-containing combinations, despite not being in the top-ranked effective combinations, could still be synergistic *in vivo* (Supplementary Fig. 3C). Given the pre-clinical data suggesting that Akt/PI3K modulation could be effective as an adjunct to BRAF inhibitors in *BRAF*-mutant melanoma (40) and the presence of an activating *PIK3CA* mutation which can predict response to PI3K/Akt/mTOR pathway inhibitors (41), we chose to test the combination of PLX4720 and Akt inhibitor perifosine (combination rank #719) in CBRC058 xenografts. Although PLX4720 had moderate single-agent activity, perifosine showed no synergistic, and even some antagonistic, interaction with PLX4720, as predicted by the *ex vivo* data (Supplementary Fig. 3C). Interestingly, this biopsy was obtained one week after the patient began treatment with a combination of BRAF and MEK inhibitors. Unfortunately, the patient's melanoma displayed intrinsic resistance to these inhibitors, with disease progression within two months of treatment initiation. This clinical resistance correlates with the lack of strong *ex vivo* or *in vivo* effect of BRAF inhibition in our tests.

In contrast to CBRC056 and CBRC058, screening of *BRAF*-mutant patient tumor CBRC026 identified a PLX4720-containing combination with the VEGFR/PDGFR inhibitor cediranib amongst the top-ranked drug combinations (Supplementary Fig. 4A). We previously discovered the combination of PLX4720 and cediranib as a novel effective combination in *BRAF*-mutant but BRAF-inhibitor-resistant melanoma cell lines (8), suggesting again that this combination could be an effective treatment in this population. We tested both this combination and one of the top–ranked combinations overall (bortezomib with dasatinib) *in vivo*. The combination of PLX4720 and cediranib showed a significant and sustained effect on tumor growth *in vivo*, as closely predicted by the *ex vivo* results (Fig.

5D). The combination of cediranib and PLX4720 reduced tumor size compared to either cediranib or PLX4720 alone ($P = 0.0156$ and $P = 0.002$, respectively, one-way ANOVA with Tukey's multiple comparison test), and significantly decreased tumor progression compared to the next most effective single drug, cediranib (Supplementary Fig. 4B, $P = 0.004$, log-rank test). The drugs were synergistic *in vivo* (19%) as identified *ex vivo* (13–30%). The combination of bortezomib and dasatinib also showed significant reduction in tumor size compared to control animals, while neither drug alone had a significant effect (Fig. 5E, $P = 0.03$, Student's *t*-test). The combination also prevented further progression of the tumor size more than dasatinib alone (Supplementary Fig. 4C, $P < 0.03$, log-rank test). The *in vivo* effect was also synergistic (23%) as predicted by the *ex vivo* data. To help understand the meaning of high versus low algorithm rankings, we also tested the much lower (#80) ranked combination of bortezomib with PLX4720. In contrast to the above data, the much lower ranked cediranib and bortezomib combination showed no added advantage over cediranib alone (Supplementary Fig. 4D).

Genetics—Ideally, novel combinatorial effects would be linked to biomarkers that could mechanistically explain the efficacy and potentially be used in clinical trials to select patients. To identify genetic biomarkers beyond *BRAF*, we used a 39 gene hotspot and tumor suppressor panel next-generation sequencing assay based on the anchored multiplex PCR (AMP) technology (32) on the tumors tested *in vivo*. Several additional mutations were identified in some of the tumors, as listed in Table 1. CBRC013 contained both GNAQ[R183Q] and NRAS[Q61H] mutations, CBRC058 contained an unusual BRAF[VK600_601>E] mutation (42), and CBRC026 contained a FGFR2[N653D] mutation. CBRC029 and CBRC056 did not contain any other hotspot mutations.

Toxicity—Drug combinations may cause unexpected additive or synergistic toxicities simultaneously with benefit from tumor shrinkage. We observed that some combinatorial activities resulted in increased systemic effects such as weight loss. Effective combinations for CBRC0013 (R788 and XL147) and CBRC029 (R788 and perifosine, tozasertib and dasatinib) led to modestly increased weight loss (Supplementary Fig. 5A–B, two-way ANOVA with repeated measures, with Tukey's correction). However, most other effective combinations, for CBRC029 (perifosine and fingolimod), CBRC056 (CX4945 and bortezomib), and CBRC026 (PLX4720 and cediranib or bortezomib and dasatinib) did not show any increased systemic toxicity from the combination of drugs compared beyond either drug alone (Supplementary Fig. 5C–E). The systemic effects of novel drug combinations were idiosyncratic to the particular combination tested and did not necessarily track with efficacy.

Discussion

In this study, we explored the feasibility of using patient biopsy material directly for high-throughput screening-based discovery of novel cancer drug combinations. There are several key advantages to this approach over previous efforts. First, we preserve tumor and stromal cell components together and score effects separately in the cancer and non-cancer cell subpopulations. Without melanoma-cell-specific segmentation (e.g., whole well ATP-based readouts), drugs with more selective tumor effects would have been missed and only drugs

with viability effects on the entire (largely non-cancerous) population would be scored as significant. Second, we were able to score results within a few days of biopsy without requiring growth of a homogenous short term culture. Even within a few passages, cancer cell populations adapt to plastic and growth media and may undergo genetic or epigenetic drift. Our data also show there are clear differences in pharmacologic vulnerabilities in the biopsies compared to long- or short-term homogenous cultures. Specific drugs, including several cytotoxic chemotherapies, show stronger effects in stable (and rapidly growing) cell lines that may overstate their effects in slower growing biopsies and within patients. Given that first-generation chemosensitivity tests require outgrowth of stable cell lines, more short-term analyses such as those utilized here may give more accurate predictive results to patients. Third, we developed a novel algorithm that incorporates the multiparametric scoring to rank new combinations. In two cases we were able to validate that lower-ranked combinations do indeed yield weaker *in vivo* responses, suggesting the algorithm ranking is predictive of both effective and ineffective combinations.

We identified a number of novel combinations of targeted therapies that subsequently showed additive or synergistic effects in PDX models of patient melanomas. In particular, we validated that cediranib, a VEGFR/PDGFR family inhibitor, has potential utility in combination with inhibitors of MAPK signaling such as vemurafenib. Additionally, we discovered novel effective combinations for further investigation including combinations with the Syk/multi-kinase inhibitor R406/R788 and PI3K/Akt inhibitors, a combination of a S1PR partial agonist and Akt inhibitor, and combinations with the proteasome inhibitor bortezomib including the CK2α inhibitor CX4945. Limited early-stage trials including bortezomib have demonstrated a few responses (43, 44), but combination regimens with targeted therapies may hold more promise based on our data. Because many of these agents have been tested in patients, clinical investigation of their utility in melanoma patients can be initiated rapidly.

Given the phenotypic nature of our screening, the mechanistic underpinnings of the combinatorial efficacy remain to be uncovered, but in some tumors additional mutations were identified by NGS that provide clear hypotheses. In patient biopsy CBRC013, we identified both *NRAS* and *GNAQ* mutations together with efficacy of a PI3K and multi-kinase inhibitor. *NRAS* mutations occur in 15–25% of all melanomas, and activation of Akt/PI3K pathway is a major consequence of *NRAS* mutations, with pathway-targeting trials underway (45). Multiple pathways are activated downstream of the G-protein coupled receptor GNAQ (46). Our data suggest kinase inhibitors like R406 may have utility in these tumors, potentially in combination with PI3K inhibitors. For patient biopsy CBRC058, PLX4720, the BRAF inhibitor in our library, did not appear in any of the top combinations, nor in the top 300 combinations. Clinically, the patient showed intrinsic resistance to dual BRAF and MEK inhibition, correlating to the observed *ex vivo* and *in vivo* responses. Next-generation sequencing identified an unusual BRAF[VK600_601>E] mutation, which may partly explain the inability of PLX4720 to inhibit growth of this tumor. For patient biopsy CBRC026, NGS identified a mutation in the RTK FGFR2. While this mutation has not been functionally annotated, it is near amino acids Tyr656 and Tyr657 conserved in FGFRs and involved in catalytic activity. Given that cediranib and to some extent, dasatinib, can have RTK inhibitory activity, it is possible that this mutation is activating and explains the kinase

inhibitor sensitivity in this patient's biopsy both *ex vivo* and *in vivo*. Combining phenotypic screening with NGS in patient biopsies could be a powerful tool for hypothesis generation and biomarker discovery.

Future studies will expand the number of biopsies to be screened and validated *in vivo* to enable broader conclusions to be reached about the predictive accuracy of the screening. Additional *in vivo* work will perform more complete dose-escalation, tolerability, and pharmacokinetic-pharmacodynamic correlation testing for drugs in our models individually and in their combination. We also will further expand analysis of the non-melanoma populations as some of the tumor-specific effects may be due in fact to modulating specific pathogenic stromal activities, such as those of cancer-associated fibroblasts (CAFs); in addition, fresh melanoma patient biopsies can contain tumor-infiltrating lymphocytes (TILs) that are functional (47), and future work will analyze their responses in the context of immuno-oncology agents. Finally, given well-documented intra-patient genetic heterogeneity, further analyses will examine functional heterogeneity from different lesions and regions of single lesions from patients, as well as follow functional responses in biopsies before, after, and while patients are on various therapies.

Even small improvements in preclinical model predictivity of clinical results can result in large improvements in drug discovery efficiency (48). New preclinical models such as patient biopsy screening described here may be more predictive than established models in cancer drug discovery. In addition to testing the feasibility of using patient biopsies as tools for combinatorial targeted therapy discovery, our study also suggests therapies identified by this method could be directed to patients on a personalized basis. While novel-novel combinations would be challenging to recommend given toxicity concerns, single agents could be readily suggested and used in the clinic. One striking feature of the results is the heterogeneity of the drug responses, in particular in the top-ranked drug combination for each patient. Individualized, precise therapies tailored to each patient may result in deeper and more durable responses to targeted therapies.

Supplementary Material

Refer to Web version on PubMed Central for supplementary material.

Acknowledgments

Grant Support: This work is funded by NIH 5R21CA175907-02 (DEF), NIH 1K08CA160692-01A1 (JAW), U54CA163125 (JAW and KTF), NIH 5P01 CA163222-04 (DEF), the Dr. Miriam and Sheldon G. Adelson Medical Research Foundation (KTF and DEF), and the Melanoma Research Alliance Team Science Award (JAW).

We thank Stewart Rudnicki and the staff of the Institute of Chemistry and Cell Biology (ICCB) – Longwood for help with UHTS screening and analysis.

References

1. Hata AN, Niederst MJ, Archibald HL, Gomez-Caraballo M, Siddiqui FM, Mulvey HE, et al. Tumor cells can follow distinct evolutionary paths to become resistant to epidermal growth factor receptor inhibition. Nat Med. 2016; 22(3):262–9. [PubMed: 26828195]

2. Ramirez M, Rajaram S, Steininger RJ, Osipchuk D, Roth MA, Morinishi LS, et al. Diverse drug-resistance mechanisms can emerge from drug-tolerant cancer persister cells. Nat Commun. 2016; 7:10690. [PubMed: 26891683]

3. Bollag G, Tsai J, Zhang J, Zhang C, Ibrahim P, Nolop K, et al. Vemurafenib: the first drug approved for BRAF-mutant cancer. Nat Rev Drug Discov. 2012; 11(11):873–86. [PubMed: 23060265]

4. Wagle N, Emery C, Berger MF, Davis MJ, Sawyer A, Pochanard P, et al. Dissecting therapeutic resistance to RAF inhibition in melanoma by tumor genomic profiling. J Clin Oncol. 2011; 29(22): 3085–96. [PubMed: 21383288]

5. Robert C, Karaszewska B, Schachter J, Rutkowski P, Mackiewicz A, Stroiakovski D, et al. Improved overall survival in melanoma with combined dabrafenib and trametinib. N Engl J Med. 2015; 372(1):30–9. [PubMed: 25399551]

6. Baselga J, Campone M, Piccart M, Burris HA 3rd, Rugo HS, Sahmoud T, et al. Everolimus in postmenopausal hormone-receptor-positive advanced breast cancer. N Engl J Med. 2012; 366(6): 520–9. [PubMed: 22149876]

7. Turajlic S, Furney SJ, Stamp G, Rana S, Ricken G, Oduko Y, et al. Whole-genome sequencing reveals complex mechanisms of intrinsic resistance to BRAF inhibition. Annals of oncology: official journal of the European Society for Medical Oncology / ESMO. 2014

8. Friedman AA, Amzallag A, Pruteanu-Malinici I, Baniya S, Cooper ZA, Piris A, et al. Landscape of Targeted Anti-Cancer Drug Synergies in Melanoma Identifies a Novel BRAF-VEGFR/PDGFR Combination Treatment. PloS one. 2015; 10(10):e0140310. [PubMed: 26461489]

9. Goodspeed A, Heiser LM, Gray JW, Costello JC. Tumor-Derived Cell Lines as Molecular Models of Cancer Pharmacogenomics. Mol Cancer Res. 2016; 14(1):3–13. [PubMed: 26248648]

10. Sandberg R, Ernberg I. The molecular portrait of in vitro growth by meta-analysis of gene-expression profiles. Genome Biol. 2005; 6(8):R65. [PubMed: 16086847]

11. Dairkee SH, Ji Y, Ben Y, Moore DH, Meng Z, Jeffrey SS. A molecular 'signature' of primary breast cancer cultures; patterns resembling tumor tissue. BMC Genomics. 2004; 5(1):47. [PubMed: 15260889]

12. Stebbing J, Paz K, Schwartz GK, Wexler LH, Maki R, Pollock RE, et al. Patient-derived xenografts for individualized care in advanced sarcoma. Cancer. 2014; 120(13):2006–15. [PubMed: 24705963]

13. Hidalgo M, Bruckheimer E, Rajeshkumar NV, Garrido-Laguna I, De Oliveira E, Rubio-Viqueira B, et al. A pilot clinical study of treatment guided by personalized tumorgrafts in patients with advanced cancer. Mol Cancer Ther. 2011; 10(8):1311–6. [PubMed: 21673092]

14. Eirew P, Steif A, Khattra J, Ha G, Yap D, Farahani H, et al. Dynamics of genomic clones in breast cancer patient xenografts at single-cell resolution. Nature. 2015; 518(7539):422–6. [PubMed: 25470049]

15. Friedman AA, Letai A, Fisher DE, Flaherty KT. Precision medicine for cancer with next-generation functional diagnostics. Nat Rev Cancer. 2015; 15(12):747–56. [PubMed: 26536825]

16. Lamothe B, Cervantes-Gomez F, Sivina M, Wierda WG, Keating MJ, Gandhi V. Proteasome inhibitor carfilzomib complements ibrutinib's action in chronic lymphocytic leukemia. Blood. 2015; 125(2):407–10. [PubMed: 25573971]

17. Tyner JW, Yang WF, Bankhead A 3rd, Fan G, Fletcher LB, Bryant J, et al. Kinase pathway dependence in primary human leukemias determined by rapid inhibitor screening. Cancer Res. 2013; 73(1):285–96. [PubMed: 23087056]

18. Masters, JRW., Palsson, B. Cancer cell lines. Vol. 1–3. Dordrecht; Boston: Kluwer Academic Publishers; 1999.

19. Zhang JH, Chung TD, Oldenburg KR. A Simple Statistical Parameter for Use in Evaluation and Validation of High Throughput Screening Assays. J Biomol Screen. 1999; 4(2):67–73. [PubMed: 10838414]

20. Mitra D, Luo X, Morgan A, Wang J, Hoang MP, Lo J, et al. An ultraviolet-radiation-independent pathway to melanoma carcinogenesis in the red hair/fair skin background. Nature. 2012; 491(7424):449–53. [PubMed: 23123854]

21. Kendrew J, Odedra R, Logie A, Taylor PJ, Pearsall S, Ogilvie DJ, et al. Anti-tumour and anti-vascular effects of cediranib (AZD2171) alone and in combination with other anti-tumour therapies. Cancer chemotherapy and pharmacology. 2013; 71(4):1021–32. [PubMed: 23355042]
22. Karabela SP, Psallidas I, Sherrill TP, Kairi CA, Zaynagetdinov R, Cheng DS, et al. Opposing effects of bortezomib-induced nuclear factor-kappaB inhibition on chemical lung carcinogenesis. Carcinogenesis. 2012; 33(4):859–67. [PubMed: 22287559]
23. Wood JM, Bold G, Buchdunger E, Cozens R, Ferrari S, Frei J, et al. PTK787/ZK 222584, a novel and potent inhibitor of vascular endothelial growth factor receptor tyrosine kinases, impairs vascular endothelial growth factor-induced responses and tumor growth after oral administration. Cancer Res. 2000; 60(8):2178–89. [PubMed: 10786682]
24. Pierre F, Chua PC, O'Brien SE, Siddiqui-Jain A, Bourbon P, Haddach M, et al. Pre-clinical characterization of CX-4945, a potent and selective small molecule inhibitor of CK2 for the treatment of cancer. Mol Cell Biochem. 2011; 356(1–2):37–43. [PubMed: 21755459]
25. Hideshima T, Catley L, Yasui H, Ishitsuka K, Raje N, Mitsiades C, et al. Perifosine, an oral bioactive novel alkylphospholipid, inhibits Akt and induces in vitro and in vivo cytotoxicity in human multiple myeloma cells. Blood. 2006; 107(10):4053–62. [PubMed: 16418332]
26. Dresang LR, Guastafierro A, Arora R, Normolle D, Chang Y, Moore PS. Response of Merkel cell polyomavirus-positive merkel cell carcinoma xenografts to a survivin inhibitor. PloS one. 2013; 8(11):e80543. [PubMed: 24260412]
27. Chakrabarty A, Sanchez V, Kuba MG, Rinehart C, Arteaga CL. Feedback upregulation of HER3 (ErbB3) expression and activity attenuates antitumor effect of PI3K inhibitors. Proc Natl Acad Sci U S A. 2012; 109(8):2718–23. [PubMed: 21368164]
28. Bahjat FR, Pine PR, Reitsma A, Cassafer G, Baluom M, Grillo S, et al. An orally bioavailable spleen tyrosine kinase inhibitor delays disease progression and prolongs survival in murine lupus. Arthritis Rheum. 2008; 58(5):1433–44. [PubMed: 18438845]
29. Wallington-Beddoe CT, Don AS, Hewson J, Qiao Q, Papa RA, Lock RB, et al. Disparate in vivo efficacy of FTY720 in xenograft models of Philadelphia positive and negative B-lineage acute lymphoblastic leukemia. PloS one. 2012; 7(5):e36429. [PubMed: 22570713]
30. Dunn EF, Iida M, Myers RA, Campbell DA, Hintz KA, Armstrong EA, et al. Dasatinib sensitizes KRAS mutant colorectal tumors to cetuximab. Oncogene. 2011; 30(5):561–74. [PubMed: 20956938]
31. Yang D, Liu H, Goga A, Kim S, Yuneva M, Bishop JM. Therapeutic potential of a synthetic lethal interaction between the MYC proto-oncogene and inhibition of aurora-B kinase. Proc Natl Acad Sci U S A. 2010; 107(31):13836–41. [PubMed: 20643922]
32. Zheng Z, Liebers M, Zhelyazkova B, Cao Y, Panditi D, Lynch KD, et al. Anchored multiplex PCR for targeted next-generation sequencing. Nat Med. 2014; 20(12):1479–84. [PubMed: 25384085]
33. Li H, Durbin R. Fast and accurate short read alignment with Burrows-Wheeler transform. Bioinformatics. 2009; 25(14):1754–60. [PubMed: 19451168]
34. Cibulskis K, Lawrence MS, Carter SL, Sivachenko A, Jaffe D, Sougnez C, et al. Sensitive detection of somatic point mutations in impure and heterogeneous cancer samples. Nat Biotechnol. 2013; 31(3):213–9. [PubMed: 23396013]
35. Fu WJ. Penalized Regressions: The Bridge versus the Lasso. Journal of Computational and Graphical Statistics. 1998; 7(3):397–416.
36. Saeed AI, Sharov V, White J, Li J, Liang W, Bhagabati N, et al. TM4: a free, open-source system for microarray data management and analysis. BioTechniques. 2003; 34(2):374–8. [PubMed: 12613259]
37. Dias-Santagata D, Akhavanfard S, David SS, Vernovsky K, Kuhlmann G, Boisvert SL, et al. Rapid targeted mutational analysis of human tumours: a clinical platform to guide personalized cancer medicine. EMBO Mol Med. 2010; 2(5):146–58. [PubMed: 20432502]
38. de Vries TJ, Smeets M, de Graaf R, Hou-Jensen K, Brocker EB, Renard N, et al. Expression of gp100, MART-1, tyrosinase, and S100 in paraffin-embedded primary melanomas and locoregional, lymph node, and visceral metastases: implications for diagnosis and immunotherapy. A study conducted by the EORTC Melanoma Cooperative Group. J Pathol. 2001; 193(1):13–20. [PubMed: 11169510]

39. Tusher VG, Tibshirani R, Chu G. Significance analysis of microarrays applied to the ionizing radiation response. Proc Natl Acad Sci U S A. 2001; 98(9):5116–21. [PubMed: 11309499]
40. Fedorenko IV, Gibney GT, Sondak VK, Smalley KS. Beyond BRAF: where next for melanoma therapy? Br J Cancer. 2015; 112(2):217–26. [PubMed: 25180764]
41. Janku F, Wheler JJ, Naing A, Falchook GS, Hong DS, Stepanek VM, et al. PIK3CA mutation H1047R is associated with response to PI3K/AKT/mTOR signaling pathway inhibitors in early-phase clinical trials. Cancer Res. 2013; 73(1):276–84. [PubMed: 23066039]
42. Voskoboynik M, Mar V, Mailer S, Colebatch A, Fennessy A, Logan A, et al. Clinicopathological characteristics associated with BRAF and BRAF mutations in melanoma. Pigment Cell Melanoma Res. 2016; 29(2):222–8. [PubMed: 26643848]
43. Markowitz J, Luedke EA, Grignol VP, Hade EM, Paul BK, Mundy-Bosse BL, et al. A phase I trial of bortezomib and interferon-alpha-2b in metastatic melanoma. J Immunother. 2014; 37(1):55–62. [PubMed: 24316557]
44. Poklepovic A, Youssefian LE, Winning M, Birdsell CA, Crosby NA, Ramakrishnan V, et al. Phase I trial of bortezomib and dacarbazine in melanoma and soft tissue sarcoma. Invest New Drugs. 2013; 31(4):937–42. [PubMed: 23315028]
45. Johnson DB, Puzanov I. Treatment of NRAS-mutant melanoma. Curr Treat Options Oncol. 2015; 16(4):15. [PubMed: 25796376]
46. Luke JJ, Triozzi PL, McKenna KC, Van Meir EG, Gershenwald JE, Bastian BC, et al. Biology of advanced uveal melanoma and next steps for clinical therapeutics. Pigment Cell Melanoma Res. 2015; 28(2):135–47. [PubMed: 25113308]
47. Ahmadzadeh M, Johnson LA, Heemskerk B, Wunderlich JR, Dudley ME, White DE, et al. Tumor antigen-specific CD8 T cells infiltrating the tumor express high levels of PD-1 and are functionally impaired. Blood. 2009; 114(8):1537–44. [PubMed: 19423728]
48. Scannell JW, Bosley J. When Quality Beats Quantity: Decision Theory, Drug Discovery, and the Reproducibility Crisis. PloS one. 2016; 11(2):e0147215. [PubMed: 26863229]

Translational Relevance

Targeted therapies can be highly effective for cancer patients, but combining them to enable durable and deep responses remains a challenge. Identifying combinations for individual patients as a precision medicine strategy requires identification of new preclinical models to rapidly discover these combinations. Stable cell lines and patient-derived xenograft (PDX) models are laborious to generate in a timeframe feasible for execution of patient-specific drug screening strategies and do not reliably include human stromal cell constituents. This study describes a next-generation chemosensitivity assay that discovers effective combinations of targeted therapies in a high-throughput and rapid manner directly from melanoma patient biopsies. In addition to identifying novel combinations that could be further developed for populations of patients, the method could also make personalized recommendations within a clinically-actionable time frame. Combining next-generation sequencing-based identification of somatic driver mutations with phenotypic screening described here could provide a more comprehensive tool for personalized medicine and efficient drug discovery.

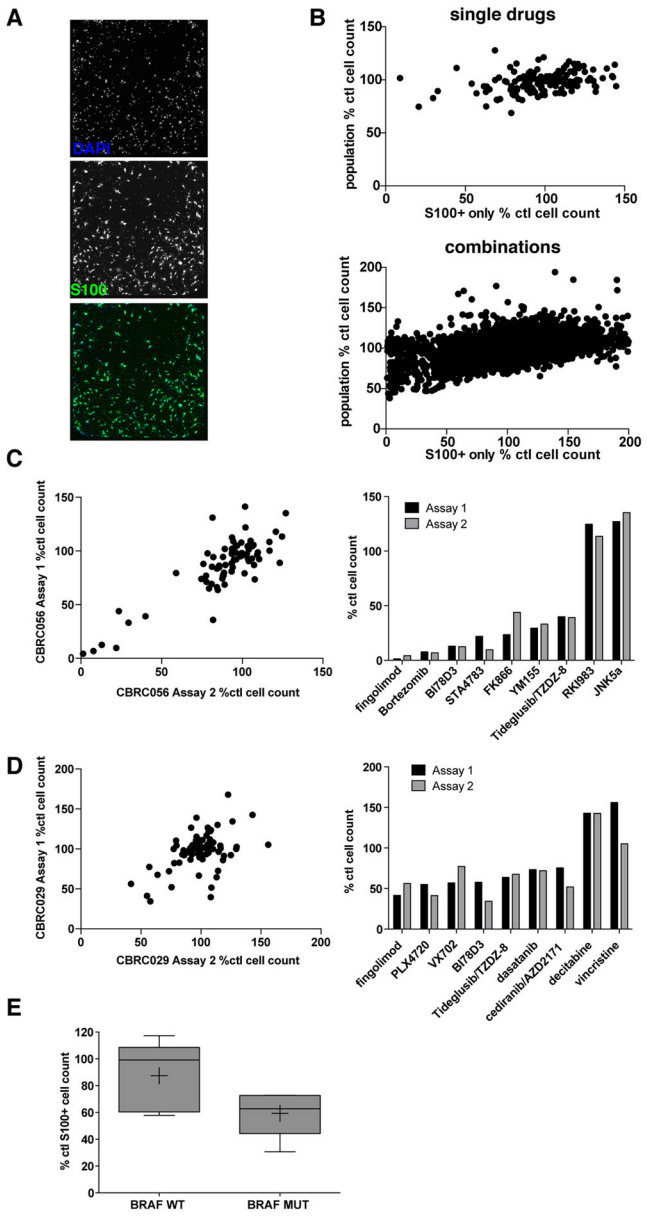

Figure 1.

A, Example images from a representative patient biopsy (CBRC013) used for automated image segmentation. Melanoma cells are marked by staining for S100 (green); all cells are marked by DAPI (blue). B, Effects of single agents (top) and all drug combinations (bottom) are plotted as percent DMSO control, comparing results for CBRC007 when only the S100+/melanoma population are scored (x-axes) versus all DAPI+ cells (y-axes). C, Comparison between technical replicates of biopsy CBRC056 single agent screening on melanoma cell population viability. D, Comparison between biological replicates of screening CBRC029 on melanoma cell population viability. E, Effect of BRAF inhibitor PLX4720 on melanoma cell viability in patient biopsies, comparing BRAF wild-type to BRAF mutant sample results.

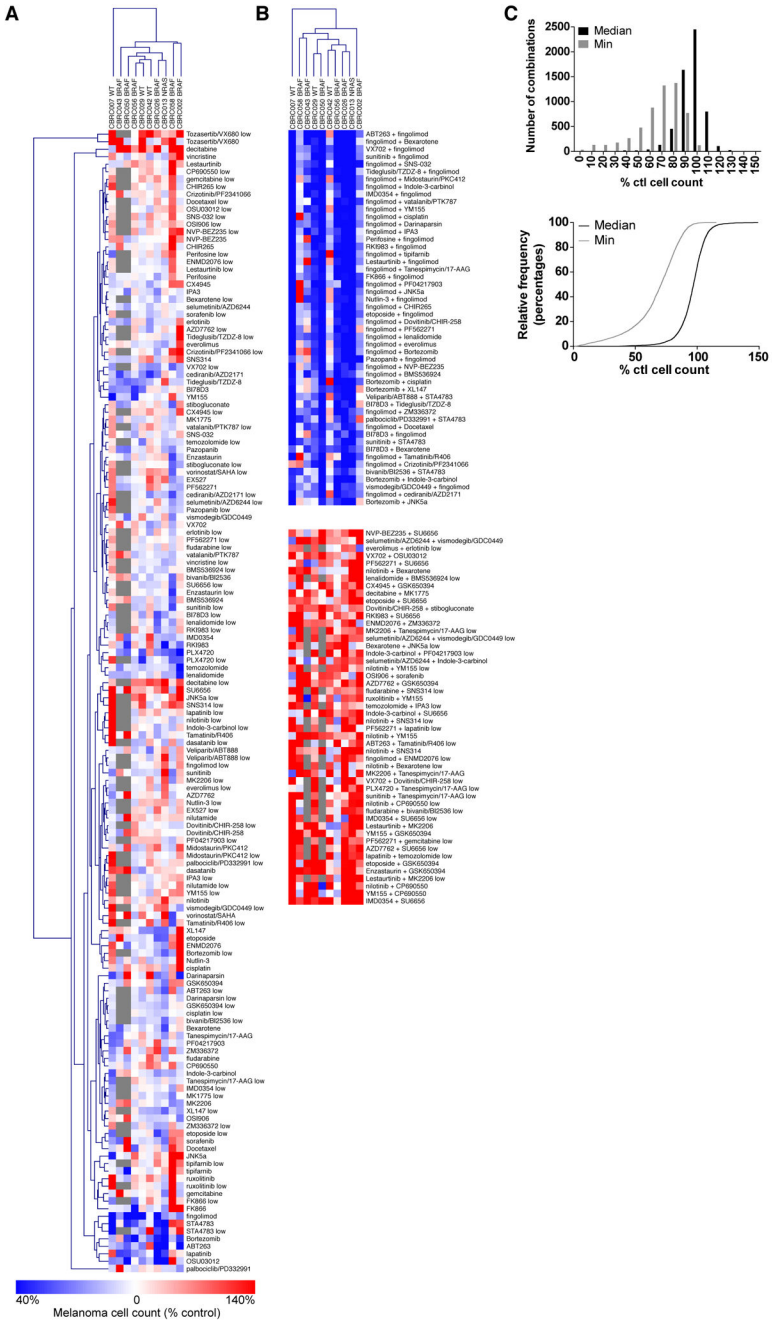

Figure 2.

A, Hierarchical clustering of single agent effects on melanoma cell viability across ten patient biopsies. B, Excerpts from hierarchical clustering of combination drug effects on melanoma cell viability across ten patient biopsies, showing significant cytotoxic (top) and pro-proliferative/anti-apoptotic (bottom) combinations. C, (Top) Binned median and minimum effects of each combination on the biopsies; while median effects of each combination were clustered at 100% control melanoma cell counts, combinations had significant effects in individual biopsies. (Bottom) Cumulative distribution of above

histogram, showing a significant percentage of combinations caused strong viability effects in only a small subset of biopsies.

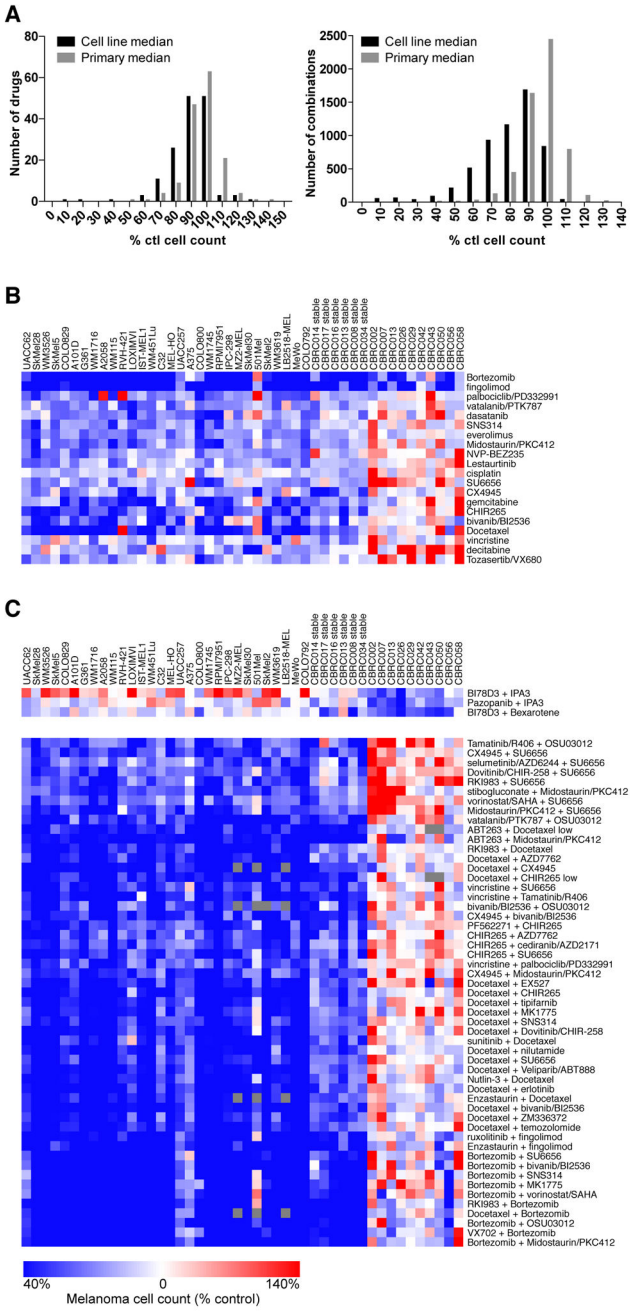

Figure 3.

A, Histogram showing the median effect of a given single agent (left) or combination of agents (right) across cell lines or primary patient biopsies. B, SAM analysis of single agents showing drugs with significant effects in cell lines but not primary biopsies. C, SAM analysis of drug combinations showing combinations with significant effects in primary biopsies but not cell lines (top) or vice-versa (bottom).

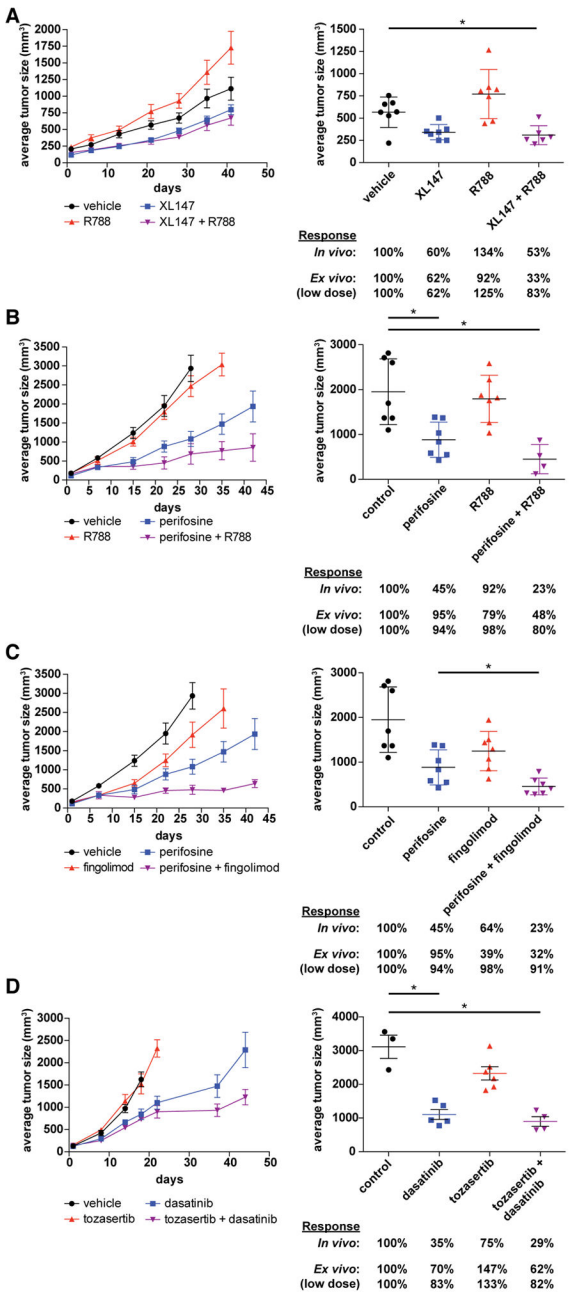

Figure 4.

A, (left) Average tumor sizes in animals treated with XL147, R788, or both ($N = 7$). Values are shown as mean +/− S.E.M. ranges. (right) CBRC013 PDX tumor sizes after three weeks of treatment. B, (left) Average CBRC029 tumor sizes in animals treated with perifosine, R788, or both ($N = 7–8$). Values are shown as mean +/− S.E.M. ranges. (right) CBRC029 PDX tumor sizes after three weeks of treatment. C, (left) Average CBRC029 tumor sizes in animals treated with perifosine, fingolimod, or both ($N = 8$). Values are shown as mean +/− S.E.M. ranges. (right) CBRC029 PDX tumor sizes after three weeks of treatment. D, (left) Average CBRC029 tumor sizes in animals treated with dasatinib, tozasertib, or both ($N = 3–$

7). Values are shown as mean +/− S.E.M. ranges. (right) CBRC029 PDX tumor sizes after three weeks of treatment.

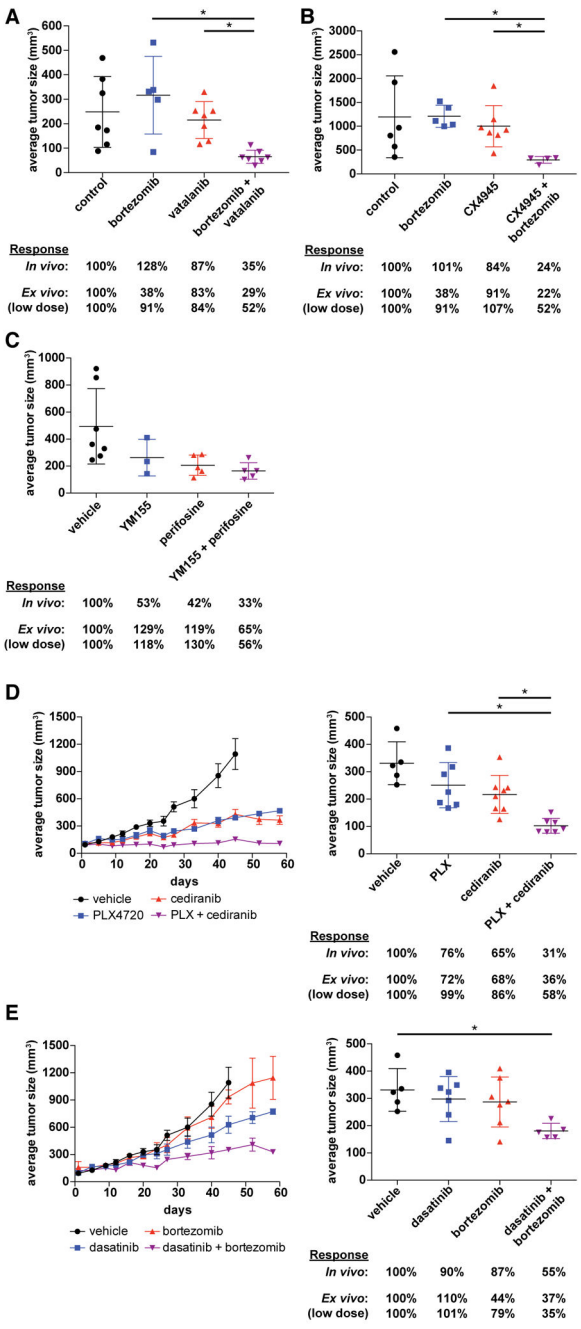

Figure 5.

A, CBRC056 PDX tumor sizes after one week of treatment ($N = 8$). B, CBRC056 PDX tumor sizes after four weeks of treatment. C, CBRC058 PDX tumor sizes after 10 days of treatment ($N = 8$) with YM155 and perifosine. D, (left) Average CBRC026 tumor sizes in animals treated with PLX4720, cediranib, or both ($N = 7–8$). Values are shown as mean +/− S.E.M. ranges. (right) CBRC026 PDX tumor sizes after three weeks of treatment. E, (left) Average CBRC026 tumor sizes in animals treated with dasatinib, bortezomib, or both ($n =$

7–8). Values are shown as mean +/− S.E.M. ranges. (right) CBRC026 PDX tumor sizes after three weeks of treatment.

Table 1

Clinical and genetic information on 10 melanoma biopsies

Patient code	Sample site	Genotype (if known)
CBRC002	Ileal metastatic mass	BRAF V600E[^]
CBRC007	Brain metastatic mass	No mutations detected[^]
CBRC013	Small bowel metastasis	GNAQ R183Q, NRAS Q61H[*]
CBRC026	Omental metastasis	BRAF V600E, FGFR2 N653D[*]
CBRC029	Axillary node from acral mass	No mutations detected[*]
CBRC042	Vulvar primary recurrence	BRAF WT[+]
CBRC043	Brain metastatic mass	BRAF Mutant[+]
CBRC050	Limb metastatic mass	BRAF V600E[^]
CBRC056	NA	BRAF V600K, PIK3CA H1047R[*]
CBRC058	NA	BRAFVK600_601>E[*]

[+] per clinical record

[^] MGH SnapShot testing (37)

[*] Hotspot NGS (32)